The April 18, 2008 Illinois Earthquake: An ANSS Monitoring Success

Robert B. Herrmann
Department of Earth and Atmospheric Sciences, Saint Louis University

Mitch Withers
Center for Earthquake Research and Information, University of Memphis

Harley Benz
National Earthquake Information Center, U.S. Geological Survey

INTRODUCTION

The largest-magnitude earthquake in the past 20 years struck near Mt. Carmel in southeastern Illinois on Friday morning, 18 April 2008 at 09:36:59 UTC (04:37 CDT). The *Mw* 5.2 earthquake was felt over an area that spanned Chicago and Atlanta, with about 40,000 reports submitted to the U.S. Geological Survey (USGS) "Did You Feel It?" system. There were at least six felt aftershocks greater than magnitude 3 and 20 aftershocks with magnitudes greater than 2 located by regional and national seismic networks. Portable instrumentation was deployed by researchers of the University of Memphis and Indiana University (the first portable station was installed at about 23:00 UTC on 18 April). The portable seismographs were deployed both to capture near-source, high-frequency ground motions for significant aftershocks and to better understand structure along the active fault. The previous similar-size earthquake within the Wabash Valley seismic zone (WVSZ) of southeastern Illinois and southwestern Indiana was a magnitude 5.0 in June 1987. The seismicity associated with the WVSZ is thought to occur in a complex horst and graben system of Precambrian igneous and metamorphic units at depths between 12 and 20 km. Paleoliquefaction evidence suggests several major shaking events have occurred within the past 12,000 years (Munson *et al.* 1997).

Table 1 lists the significant earthquakes in this part of southeastern Illinois and southwestern Indiana. The locations with intensities are from a catalog of Nuttli and Brill (1981). The location of most earthquakes in the 1900s benefited from the increasing number of seismograph stations in the area. The recurrence rate of the significant events is roughly one every 10 years. The distinctive difference between the earlier earthquakes and the 18 April mainshock is the presence of modern digital instruments near the earthquake source, which permits improved location and, for the first time, rapid determination of moment tensor solutions for several aftershocks.

NEIC RESPONSE

Since USGS Circular 1188 was published in 1999 (USGS 1999) outlining an Advanced National Seismic System (ANSS), significant improvements have been made in terms of seismic monitoring infrastructure, coordinated network operations, and distribution of earthquake information products. Annual highlights are given at the link http://earthquake.usgs.gov/research/monitoring/anss/milestones.php.

Some important milestones in the development of integrated seismic monitoring in the United States are the deployment of significant numbers of strong-motion systems in the central U.S. in 2001–2003, establishment of the National Earthquake Information Center (NEIC) 24/7 operations in 2006, and implementation of the Prompt Assessment Of Global Earthquakes For Response system (PAGER; http://earthquake.usgs.gov/pager) in 2007. In the central Mississippi Valley region, the ANSS effort provided new broadband/strong-motion stations, upgrades to other sites, and new digital accelerographs.

Throughout the central United States, NEIC coordinates earthquake response with the Center for Earthquake Research and Information (CERI) at the University of Memphis and with Saint Louis University (SLU). NEIC primarily relies on real-time broadband stations of the ANSS backbone network and those operated by CERI and SLU. The backbone stations ensure a uniform monitoring capability for the region to approximately magnitude **M** 3.0 or larger, while the regional broadband stations operated by CERI and SLU provide additional details on seismic activity to approximately **M** 2.0 or larger in active source zones (*e.g.*, the New Madrid seismic zone) within the central United States.

For the **M** 5.2 Illinois event, NEIC provided the initial earthquake notification and response information. The NEIC automatic system had a primary location and magnitude in approximately 2 m 30 s after origin time (OT). An NEIC analyst-reviewed location and magnitude (38.57N, 87.89E, *M* 5.4)

doi: 10.1785/gssrl.79.6.830

TABLE 1
Significant Earthquakes in the Wabash Valley Seismic Zone

Date	Time	Lat (N)	Lon (W)	H (km)	MMI or Mw	Stk	Dip	Rake	Ref.
18380609	14:45	38.5	89.0		VII–VIII				1
18760925	06:15	38.5	87.8		VI				1
18870206	22:15	38.7	87.5		V–VI				1
18910927	04:55	38.3	88.5		VII				1
18990430	02:05	38.5	87.0		VI–VII				1
19090927	19:00	38.7	88.4		VII				1
19221127	03:31	37.8	88.5		VI–VII				1
19250427	04:05	38.3	87.6		VI–VII				1
19250902	11:55	37.8	87.5		VI				1
19581108	02:41:12	38.44	88.01		VI				1, 7
19681109	17:01:42	37.91	88.37	22	5.29	0	46	79	3
19740403	23:05:02	38.55	88.07	15	4.34	310	70	0	3
19870610	23:48:55	38.71	87.95	10	4.96	135	70	15	4
20020618	17:37:17	37.99	87.87	19	4.50	120	80	10	2, 5
20080418	09:37:00	38.45	87.89	14	5.23	25	90	–175	2, 6
20080418	15:14:16	38.48	87.89	14	4.61	225	80	–180	2, 6
20080421	05:38:30	38.47	87.82	15	4.00	210	85	175	2, 6
20080425	17:31:00	38.45	87.87	13	3.72	295	80	5	2, 6
20080605	07:13:15	38.45	87.87	17	3.37	305	90	20	2,6

1 Nuttli and Brill (1981); 2 http://www.eas.slu.edu/Earthquake_Center/MECH.NA/ ; 3 Herrmann (1979); 4 Taylor *et al.* (1989); 5 Kim (2003); 6 This study; 7 Gordon (1983).

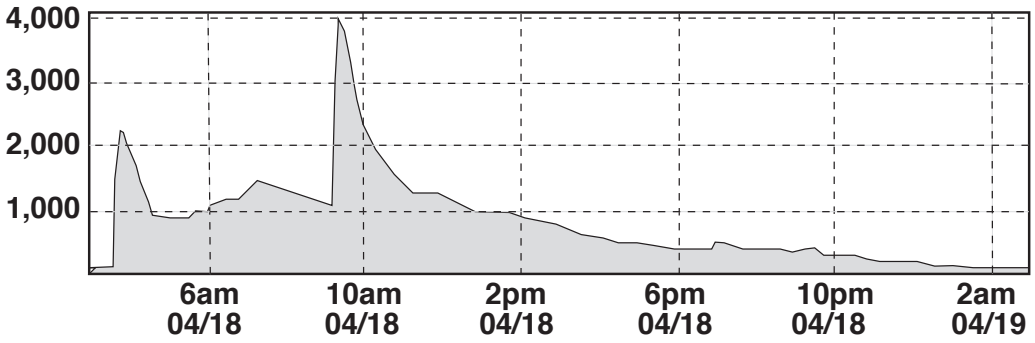

▲ **Figure 1.** NEIC edge server response April 18–19, 2008, showing the number of hits per second. There were approximately 68 million hits in the 24 hours after the earthquake. The peak rate was 3,892 hits/s at 09:20 Mountain Daylight time (MDT). All times are given in MDT (UTC –6).

was released in 15 m 53 s after OT. This was followed up at 1 h 23 m after OT with a revised location and magnitude (38.48N, 87.83W, *Mw* 5.2) based on the regional moment tensor solution and re-analysis of seismic arrival times and supplemental seismic data. A final location (38.45N, 87.89W) was contributed by CERI at 2 h 2 m after OT, based on CERI analysis using an appropriate local velocity model and additional arrival time information.

Public information is distributed through the Earthquake Hazards Program servers (EHPs). The access statistics are interesting. Figure 1 shows the number of hits per second for the 24-hour period containing the *Mw* 5.2 earthquake and its *Mw* 4.6 aftershock. The main event occurred in the early morning, but the increased awareness at the time of the aftershock led to a high hit rate. These statistics are important since they highlight the importance of having the proper support infrastructure to provide information to an increasing wired public.

As expected, public interest in the earthquake led to a well-defined felt map for the main event and seven aftershocks. The intensity map for the mainshock, based on "Did You Feel It?" (DYFI) responses, is shown in Figure 2. This map highlights the observations of strongest shaking near the epicenter, with

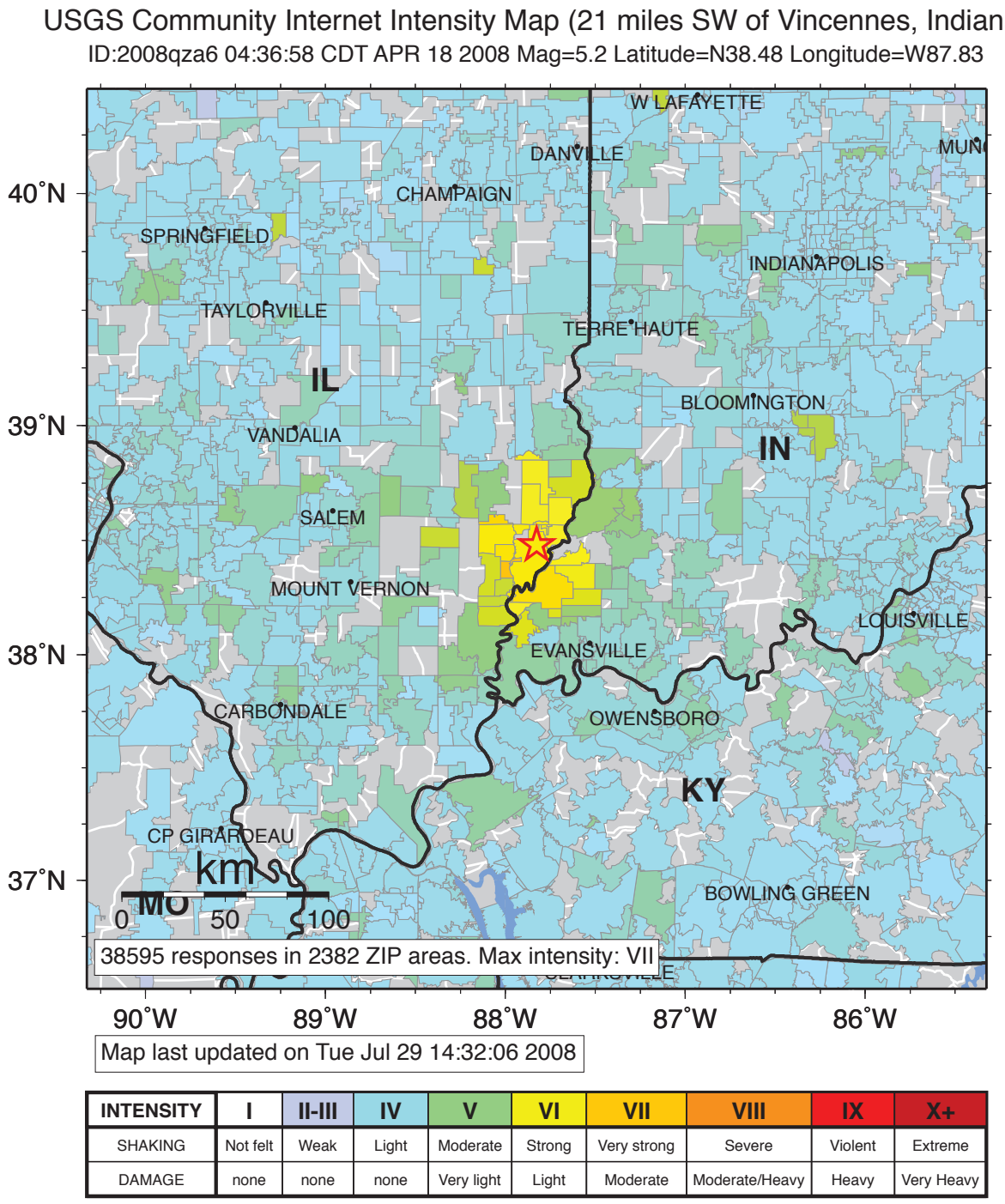

INTENSITY	I	II-III	IV	V	VI	VII	VIII	IX	X+
SHAKING	Not felt	Weak	Light	Moderate	Strong	Very strong	Severe	Violent	Extreme
DAMAGE	none	none	none	Very light	Light	Moderate	Moderate/Heavy	Heavy	Very Heavy

▲ **Figure 2.** NEIC "Did You Feel It?" map showing the responses for the April 18 main earthquake at 0937. There were 41,128 responses.

felt information provided by people in 2,381 ZIP Codes in 17 states. An important feature seen in the map is the lack of reports from some ZIP Codes near the epicenter, which reflects the rural nature of some areas as much as the lack of felt intensities. Such reporting gaps may also appear in the felt reports of previous earthquakes. Approximately 75% of the total number of DYFI responses occurred within eight hours of OT, and the final DYFI reports came in over the next 24 hours, primarily influenced by local news reports and media information on earthquake links. Combined, the total number of DYFI responses for the mainshock and the seven largest aftershocks (magnitude range **M** 3.1–4.6) totaled 54,321 responses.

EARTHQUAKE SEQUENCE

A tabulation of earthquakes located by the permanent network is given in Table 2. The epicenters are plotted in Figure 3 together with the moment tensor solutions obtained for the five largest events. The main features of the earthquake locations are an approximately east-west trend of aftershocks with depths between

TABLE 2
Network Locations of Earthquakes in the Sequence

Year	Mo	Dy	Hr	Mn	Sec	Lat	Lon	H (km)	Mag	Nph	Gap	Dmin	RMS	Q	Az	Dip	Len	Az	Dip	Len
2008	04	18	09	36	59.1	38.450	–87.890	14.2	5.20	22	86	9	0.2	B	164	16	1.3	268	40	1.8
2008	04	18	10	03	59.6	38.450	–87.860	13.4	2.20	15	89	7	0.16	B	165	1	0.8	74	22	2.4
2008	04	18	10	06	06.1	38.440	–87.880	19.1	1.90	8	130	8	0.17	B	183	22	2.1	73	40	3.8
2008	04	18	10	15	31.4	38.450	–87.840	16.4	1.60	11	111	6	0.05	B	168	7	1.9	264	41	3.4
2008	04	18	10	36	32.8	38.460	–87.870	18.3	2.50	17	89	8	0.17	A	340	1	1.8	71	45	1.5
2008	04	18	10	37	26.4	38.480	–87.860	14.2	2.10	7	133	9	0.12	C	341	8	2.2	248	18	4.1
2008	04	18	10	44	10.6	38.450	–87.850	16.1	1.60	11	134	7	0.21	B	168	4	2.5	75	37	2.4
2008	04	18	10	46	24.0	38.440	–87.880	17.8	2.20	15	86	8	0.17	A	26	23	1.5	127	25	0.8
2008	04	18	10	57	47.4	38.430	–87.920	17.2	1.50	13	124	12	0.24	B	25	16	1.7	124	28	2.2
2008	04	18	11	25	25.5	38.450	–87.870	15.3	1.20	12	115	9	0.09	B	346	0	0.8	76	19	2
2008	04	18	11	55	57.6	38.440	–87.880	14.2	2.70	16	85	9	0.11	B	346	0	0.8	256	22	2.5
2008	04	18	15	14	17.2	38.460	–87.870	15.5	4.60	25	89	8	0.28	A	54	27	1	308	28	1.2
2008	04	19	03	05	53.2	38.440	–87.890	14.3	2.70	15	105	9	0.17	B	162	1	0.7	72	24	1.5
2008	04	19	09	46	43.5	38.440	–87.850	14.4	1.30	12	113	7	0.11	B	146	3	1.2	54	34	1.9
2008	04	19	12	45	37.7	38.450	–87.910	15.4	1.70	13	121	11	0.15	B	349	0	0.8	80	23	1.7
2008	04	19	16	55	17.2	38.440	–87.900	14.5	2.80	16	103	10	0.12	B	346	0	0.8	76	21	2
2008	04	20	05	02	41.7	38.440	–87.850	16.2	2.80	16	88	6	0.12	A	156	6	1.1	63	29	1.7
2008	04	20	05	31	42.4	38.450	–87.880	14.4	1.70	12	131	9	0.13	B	154	1	1.2	64	17	2.2
2008	04	20	06	32	02.3	38.440	–87.840	16.5	1.00	11	134	6	0.18	B	159	10	1.9	63	28	2.2
2008	04	20	09	59	44.3	38.460	–87.840	13.8	1.30	11	136	6	0.2	B	147	9	1.9	51	33	2.6
2008	04	20	10	34	26.0	38.440	–87.900	17.1	2.30	15	120	10	0.13	A	4	3	1.5	96	29	2.1
2008	04	21	05	38	30.3	38.450	–87.880	18.3	4.00	20	87	8	0.15	A	9	16	0.7	109	30	0.8
2008	04	21	07	58	45.5	38.450	–87.880	17.2	2.20	16	86	9	0.22	A	81	8	2.2	173	14	1.9
2008	04	21	09	45	11.5	38.440	–87.900	17.1	1.20	11	120	10	0.22	B	8	7	1.7	100	17	2.7
2008	04	22	08	01	00.1	38.460	–87.900	13.7	1.60	11	119	11	0.08	B	148	7	0.9	53	36	2.7
2008	04	23	01	32	33.5	38.450	–87.880	16.6	2.10	13	116	9	0.12	B	144	6	1.2	49	37	1.9
2008	04	24	11	44	24.4	38.450	–87.900	18.3	2.60	18	85	11	0.12	A	165	3	0.8	74	26	1.7
2008	04	25	17	31	00.5	38.450	–87.870	13.0	4.20	16	87	8	0.15	A	154	2	0.8	63	25	1.8
2008	04	28	21	46	59.0	38.450	–87.850	14.1	1.70	11	134	6	0.16	B	13	24	2	120	33	2.1
2008	04	30	19	29	18.8	38.450	–87.870	15.4	2.60	16	87	8	0.14	B	167	1	0.8	76	19	2
2008	05	01	05	30	37.7	38.450	–87.860	14.3	3.30	19	89	7	0.2	A	343	1	0.8	73	11	1.7
2008	05	03	00	34	19.5	38.450	–87.860	16.1	1.40	9	113	7	0.06	B	341	13	1.7	243	31	3.6
2008	05	29	10	49	27.6	38.440	–87.860	14.0	2.00	16	87	7	0.36	A	85	5	1.8	353	18	1.7
2008	06	01	14	56	12	38.453	–87.852	14.2	1.6	14	112	7	0.23	B	10	18	1.75	113	35	2.0
2008	06	05	07	13	15.5	38.448	–86.867	16.2	3.37	17	135	6	0.16	A	149	7	0.72	55	31	0.9
2008	06	24	22	20	09.5	38.449	–87.864	14.6	2.9	16	88	7	0.21	A	160	3	0.73	253	39	1.2

The shaded entries indicate earthquakes with moment tensor solutions.

13 km and 20 km. This spatial distribution is similar to that of the 10 June 1987 earthquake and its aftershocks (Taylor *et al.* 1989).

MOMENT TENSOR SOLUTIONS

Considerable efforts have been made to compute moment tensor solutions for events with **M** > 3.5 for most of North America (http://www.eas.slu.edu/Earthquake_Center/MECH.NA). Two techniques are used: direct inversion of broadband waveforms out to an epicentral distance of 500 km, and a fit to the surface-wave spectral amplitude radiation pattern (Herrmann 1979b). The latter technique depends less upon the particular velocity model used, but requires other information, such as *P*-wave first motion data or a match between an observed and predicted waveform to resolve the ambiguities due to fitting just the fundamental mode surface-wave radiation patterns of Love waves and Rayleigh waves.

For this region of the central United States we use the simple CUS velocity model described by Wang and Herrmann (1980) to create the Green's functions used for the waveform moment

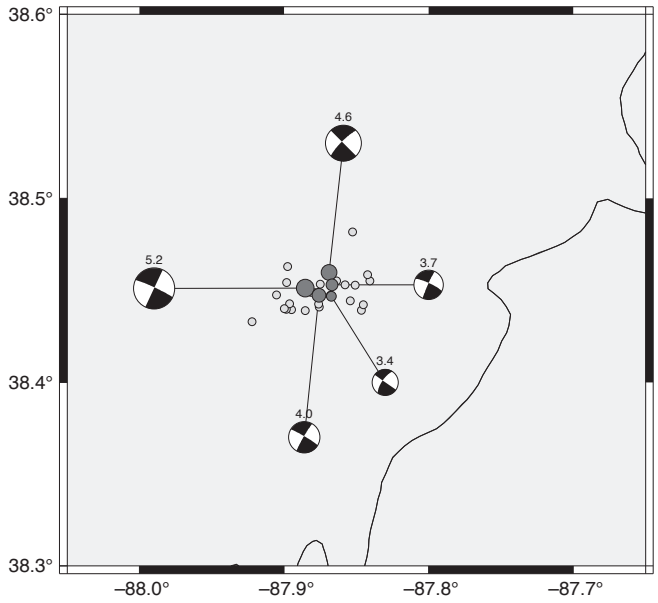

▲ **Figure 3.** Earthquakes located by the permanent network (small dots) and larger earthquakes (large dots) having broadband moment tensor solutions.

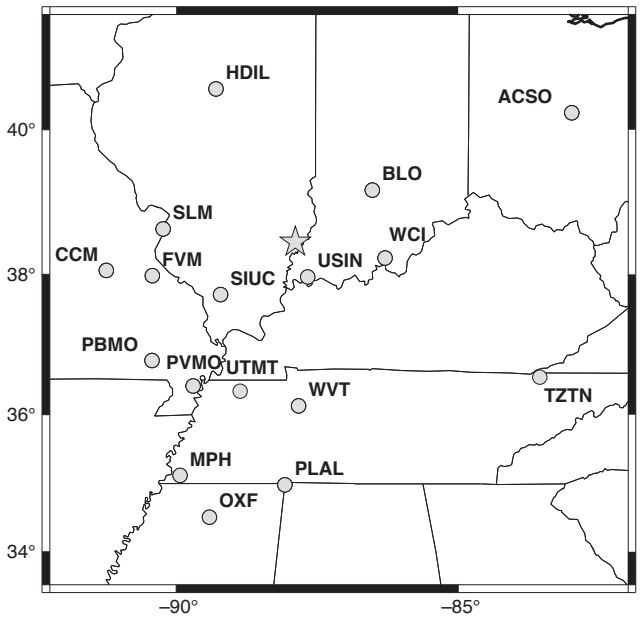

▲ **Figure 4.** Location of broadband stations used in the moment tensor inversion for the main event.

tensor inversion and the eigenfunctions for the surface-wave spectral amplitude study. We used the inversion procedures and codes described in Herrmann and Ammon (2002).

Data processing for the waveform inversion consisted of a deconvolution to ground velocity in units of *m/s* and a quality control check on the resultant waveforms, followed by a grid search over the focal mechanism parameters of strike, dip, and rake angles and source depth. Both the observed ground velocities and the Green's function velocities were filtered between 0.02 and 0.10 Hz using three-pole Butterworth highpass and lowpass filters, respectively. We use a wide frequency band and ground velocity to preserve sufficient detail of the data to permit a qualitative evaluation of the appropriateness of the crustal model used. We did not use the "cut-and-paste" method of Zhu and Helmberger (1996) since we normally do not see the *P*- or *S*-wave phases clearly for smaller events and since the velocity model use is more than adequate to model the entire wavetrain.

Figure 4 shows the location of the mainshock and the broadband stations used for the source inversion. Many of the stations shown in Figure 4 were strategically installed at their locations to provide good sampling in azimuth and distance for improved earthquake monitoring in the Wabash Valley and other active areas in the region.

Figure 5 shows a comparison of the observed and predicted waveforms for the 18 April 0937 main event. Except for the transverse component at USIN, which may be affected by being near a node in the radiation pattern, the fits are superb. The simple velocity model adequately describes the surface-wave pulse as well as the *P*, *sP*, and *S* arrivals.

Figure 6 shows the locations of 579 broadband stations in North America, which provided waveforms for the determination of the focal mechanism, depth, and moment magnitude from the fundamental mode Love- and Rayleigh-wave radiation patterns. Although the source parameters were well-defined by the inversion of regional broadband waveforms, the surface-wave study was done for completeness. Group velocities and spectral amplitudes are obtained through the application of a multiple filter technique (Dziewonski *et al.* 1969; Herrmann 1973). The data preparation provided 40,000 group velocity dispersion points to an existing database of more than 400,000 dispersion observations in a separate continental surface-wave tomography study. The spectral amplitude information also can be used for continental attenuation studies.

Figure 7 compares selected observed and predicted spectral amplitudes at periods of 10, 20, and 50 s for both the Love and Rayleigh waves. The inversion program compares observed and predicted spectral amplitudes, which down-weights observations at large distances that can be affected by focusing and differences in the attenuation model. The observations in Figure 7 are corrected to the source for Q and the geometrical spreading to a reference distance of 1,000 km. Since the dataset is dominated by contributions from the National Science Foundation (NSF)–supported Transportable Array (http://www.earthscope.org), attenuation differences cause the apparent lack of good fit to the west at shorter periods.

The moment tensor solution parameters for five earthquakes in this sequence are provided in Table 1, and the focal mechanisms are shown in Figure 8. Of these earthquakes, the smallest had the least number of observations and required careful selection of waveforms and changes in normal bandpass filters to obtain a solution. The other solutions are well-determined. In all cases, the pressure axes trend in an east-west direction and the depths vary from 13 to 17 km. The strikes of the nodal planes are slightly different, especially those of the 18 April 15:14 aftershock. An examination of the inversion results for that earthquake indicates that the difference is real.

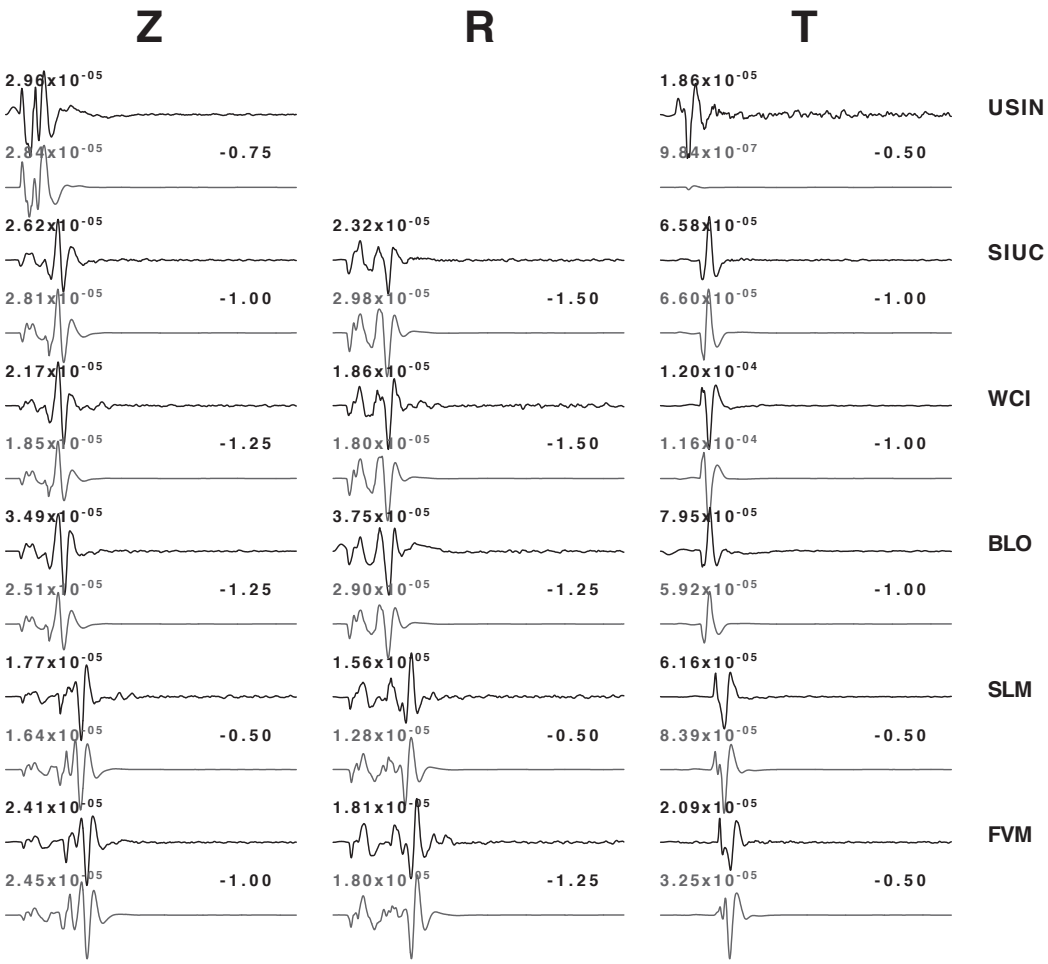

▲ **Figure 5.** Comparison of observed (black) and predicted (gray) waveforms for the main event at stations out to distances of 260 km. The inversion used all stations shown in Figure 4, which provided data to 460 km. Each observed-predicted trace pair is plotted to the same scale, with the peak amplitude of the filtered ground velocity indicated. Each trace starts 10 s before the *P*-wave arrival and continues to 180 s after *P*. The single number plotted between each trace pair indicates the time shift required to align the Green's function for the best fit; the shift depends on the ability to pick the first *P*-wave arrival correctly, the granularity of the Green's functions, which were computed with a 0.25 s sampling interval, and the adequacy of the velocity model.

HIGH-FREQUENCY GROUND MOTION

As a result of the installation of ANSS strong-motion instrumentation in the region before 2005, the 18 April 09:37 earthquake provided the first well-recorded strong-motion dataset for the central and eastern United States. Instrumentation consisted of Guralp CMG-5TD accelerometer/digitizer and Kinemetrics EpiSensor/Quanterra 330 accelerometer/digitizer combinations recording at 50 Hz and 100 Hz, respectively. The nearest instrument was at the Wabash Valley College in Mt. Carmel, Illinois, at an epicentral distance of 9.6 km (hypocentral distance of 17.0 km). In addition to the accelerographs, 24-bit broadband sensors provided additional information for ground velocity and acceleration.

Figure 9 shows the locations of 24-bit digital recordings of the main event in the region. The closest was in Mt. Carmel, Illinois, (WVIL, epicentral distance of 9.7 km) and the farthest was in Charleston, South Carolina.

To test the possible use of the data for ground-motion scaling studies, we carefully deconvolved all digital data to ground velocity in m/s. To estimate ground acceleration, the velocity time series were differentiated using a one-sided difference operator. The peak values of the vertical (Z), radial (R), and transverse (T) components were noted and plotted as a function of epicentral distance. Figures 10 and 11 are plots of the peak ground accelerations and velocities, respectively. For reference, we also plotted the hard-rock prediction for the Atkinson and Boore (1995) model for an $Mw = 5.23$ source with an assumed source depth of 15 km. There was no attempt to distinguish different site conditions. We note that some sites are on Paleozoic hard rock and other sites are on softer soils and sediments, which are in the process of being characterized through shallow geophysical investigations (Odum *et al.* 2005; Odum *et al.* 2008).

The interesting features of these figures are the number of observations for just one central U. S. earthquake and the sim-

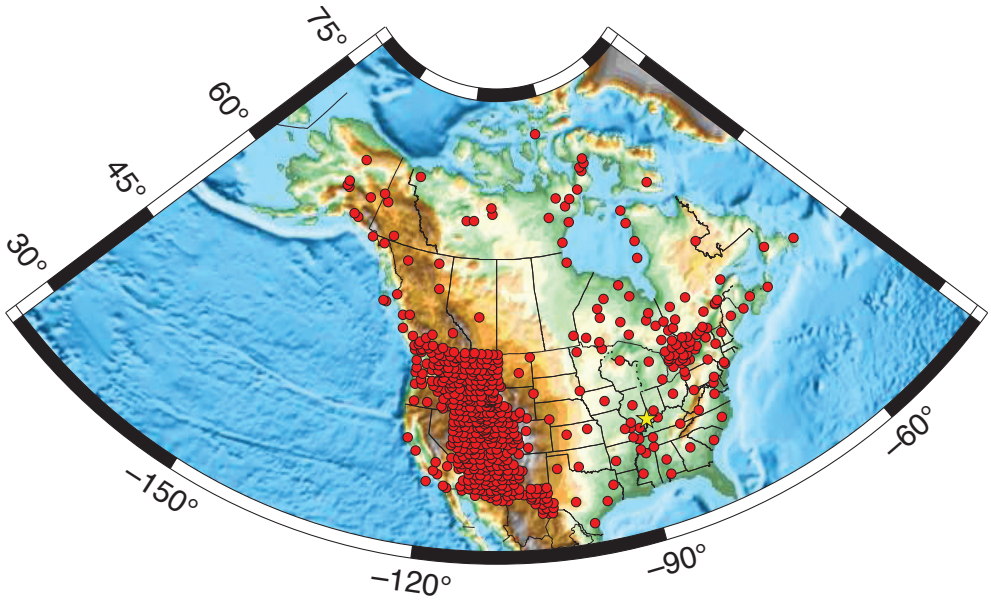

▲ **Figure 6.** Location of stations in North America used to determine the focal mechanisms from the surface-wave spectral amplitude radiation pattern. The stations include those of Natural Resources Canada, the USGS and USGS supported networks, and NSF-supported Transportable Array.

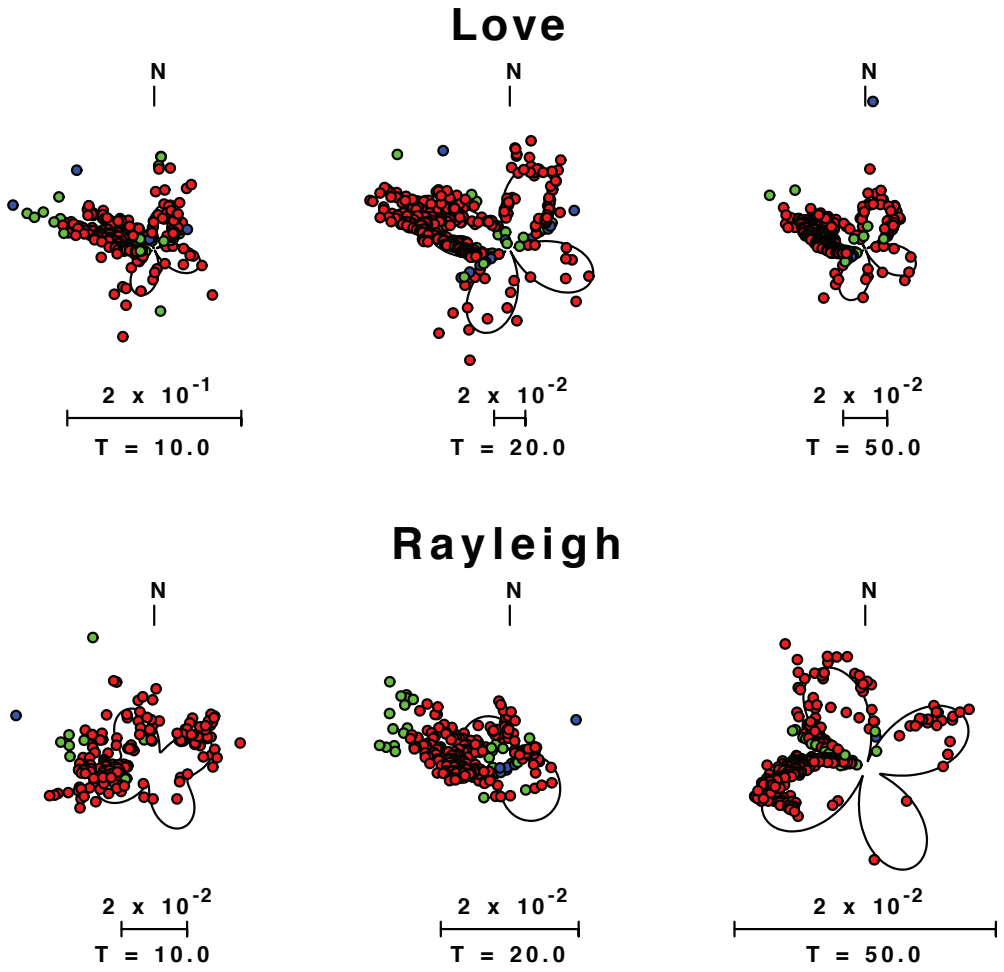

▲ **Figure 7.** Comparison of *Q*-corrected observed (colored dots) and predicted (solid curve) Love and Rayleigh spectral amplitude radiation patterns at a distance of 1,000 km for selected periods. The scale indicates the spectral amplitudes in units of cm-s.

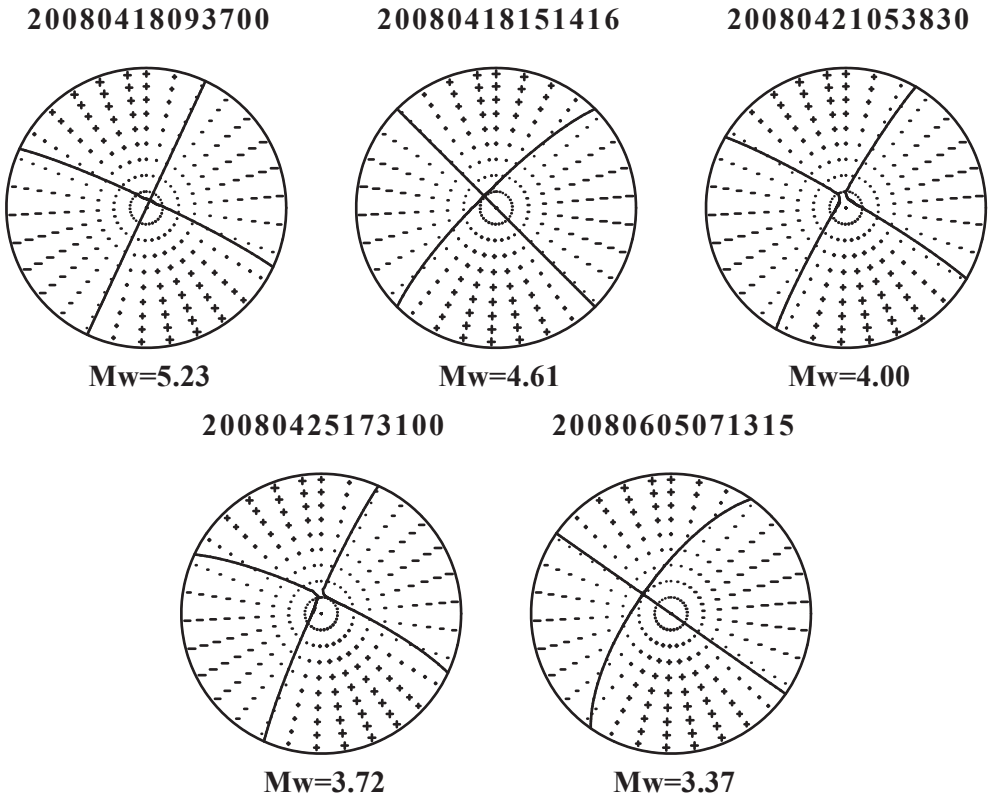

▲ **Figure 8.** Focal mechanisms derived from inversion of broadband waveforms. The origin time and moment magnitude is plotted for each solution. The plus and minus symbols indicate the theoretical *P*-wave first motion amplitudes and polarities for the given mechanism.

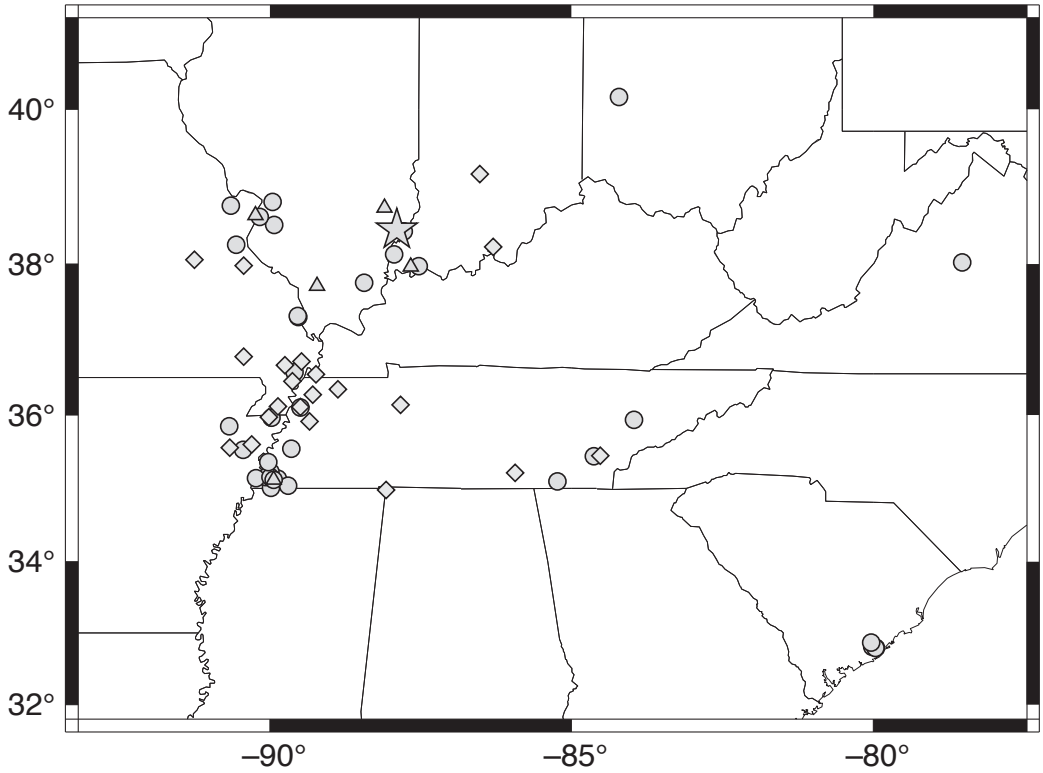

▲ **Figure 9.** Location of ANSS stations used for peak ground-motion study. The star indicates the epicenter. Stations with only an accelerometer are indicated by a triangle, those with only a broadband sensor by a diamond, and stations with both channels by a circle.

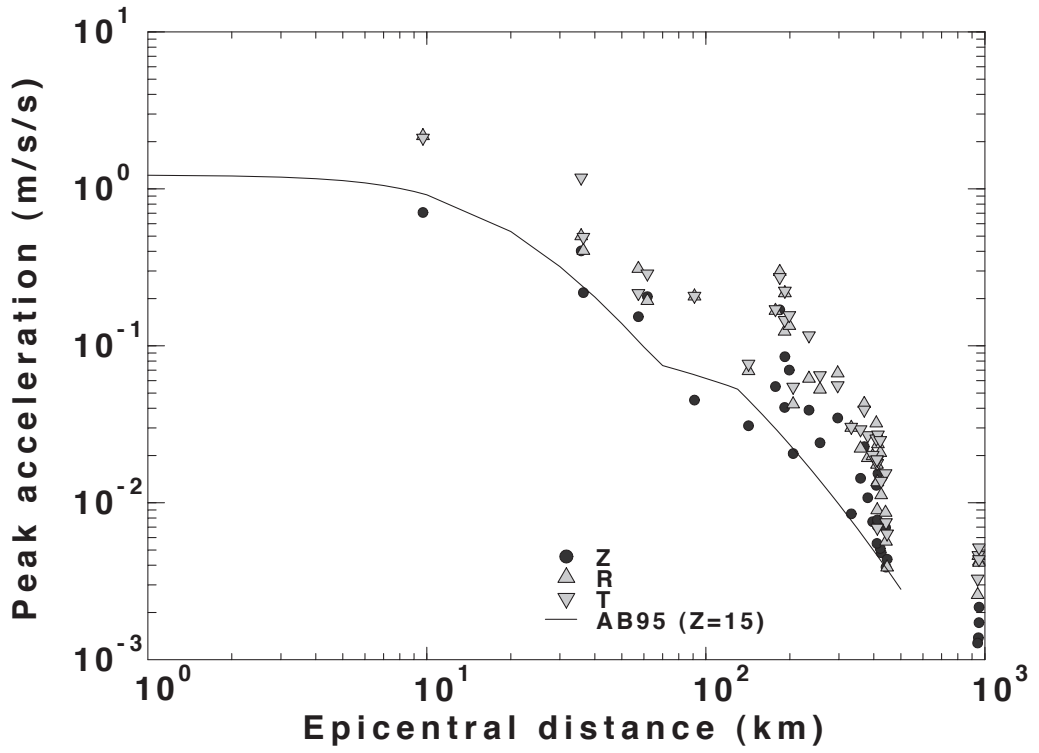

▲ **Figure 10.** Comparison of observed peak ground acceleration and predicted hard-rock values (AB95: Atkinson and Boore 1995) for an *Mw* = 5.23 earthquake. Different symbols are used to indicate the component of motion.

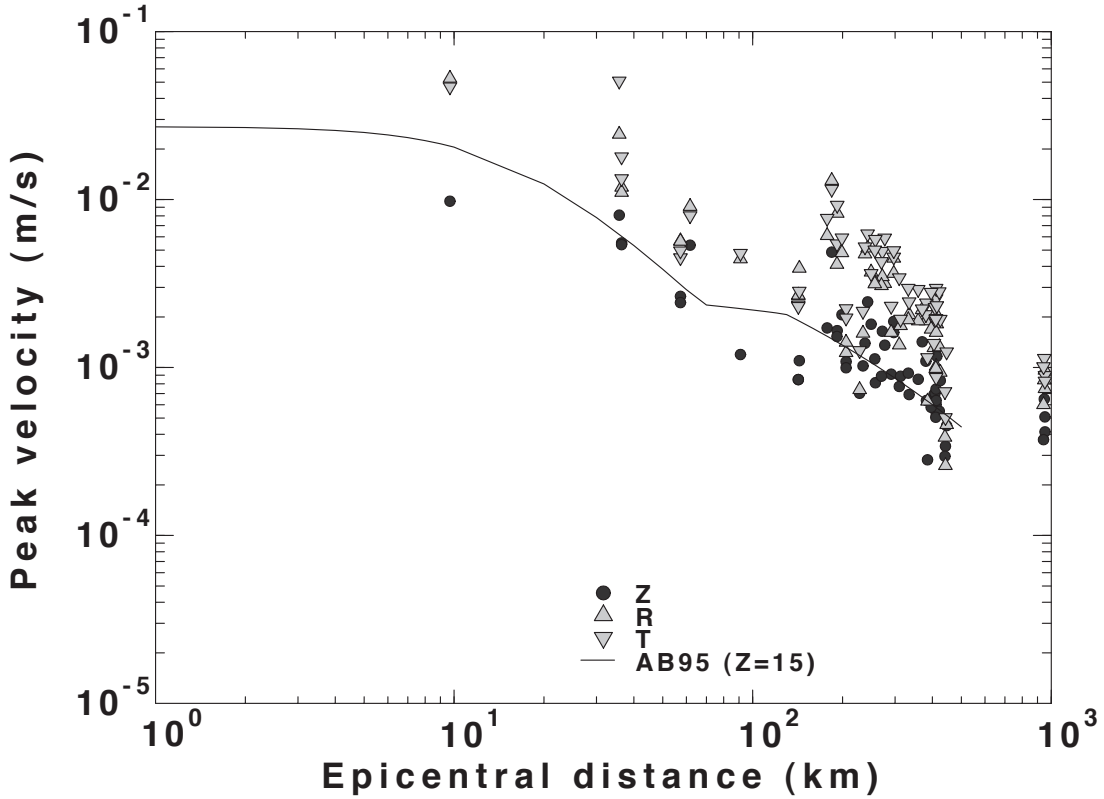

▲ **Figure 11.** Comparison of observed peak ground velocity and predicted hard-rock values (AB95: Atkinson and Boore 1995) for an *Mw* = 5.23 earthquake. Different symbols are used to indicate the component of motion.

ilarity of the peak motions on the vertical component to the Atkinson and Boore (1995) hard rock predictions. Although the $Mw = 5.23$ earthquake was not large enough to address questions about large earthquake ground motions in the region, it does provide data to compare distance scaling and absolute source scaling models up to this moment magnitude.

SOURCE SCALING

Because of the large number of well-recorded and located earthquakes and the presence of stations near the earthquake source, we can quickly evaluate the suitability of using the digital datasets for source scaling studies. The aftershock locations are tightly clustered, and the epicentral distance to the nearest broadband station, OLIL, varies between 33.5 km and 37.7 km for the five events that have a well-determined moment magnitude and source mechanism. We will apply a coda normalization technique to the horizontal recordings at OLIL to estimate absolute source scaling. Coda normalization was introduced by Aki (1980) and used by Frankel *et al.* (1990) and Mayeda *et al.* (2003). The concept is that the event coda consists of shear waves scattered by crustal and upper mantle heterogeneities. At large lag times, the coda provides a complete sampling of the source radiation pattern. In the special case of fixed source and station locations, changes in the coda level in a narrow frequency window are assumed to be directly related to shear-wave generation by the source. We followed Mayeda *et al.* (2003) for signal processing, but skipped several of his calibration steps because of the fixed locations.

As part of routine processing, the original signals were corrected for instrument response to yield ground velocity in units of m/s. We then removed the mean, bandpass-filtered the trace by applying a four-pole Butterworth highpass filter followed by a four-pole Butterworth lowpass filter, reversed the time series, reapplied the same filters, and then reversed the time series again to implement a zero-phase bandpass operation. We used the filter corners of 0.07–0.10, 0.10–0.20, 0.20–0.30, 0.30–0.50, 0.50–0.70, 0.70–1.00, 1.0–2.0, 2.0–3.0, 3.0–5.0, 5.0–7.0, 7.0–10.0, 10.0–20.0, and 20.0–30.0 Hz. The time domain amplitudes were divided by the filter bandwidth and a center frequency was defined as the mean of the two corners. The signal envelope was formed, a $\log_{10}$ was taken, and a mean operator with half-width of eight samples was applied to smooth the envelope. Finally the envelopes of the radial and transverse components were averaged. Figure 12 shows the envelopes for the five earthquakes filtered in the 10–20 Hz band. The plots start from 40 s before to 110 s after the origin time. Note that events 3 and 4 ($Mw = 4.00$ and 3.73, respectively) overlie each other in the 10–20 Hz band.

To define a stable level, we determined the envelope mean level in a window 90–110 s after the origin time and used the mean signal at times 30–40 s before the origin time to represent a noise estimate. We accepted the signal coda level if it was 0.3 log units above the pre-event noise estimate. Figure 13 gives a plot of the mean coda envelope levels using this procedure. The shift of the levels between the events is related directly to the differences in the spectral content at the source, because the same site and propagation effects are common to all five curves in Figure 13.

The coda-normalization ties the differences in the coda levels to differences in source spectrum. We assume that the source moment-rate spectrum (the far-field body wave spectrum) varies as f^0 at frequencies $<< f_c$ and as f^{-2} for frequencies $>> f_c$, where f_c is the corner frequency for a given seismic moment. Because of this assumption, the coda amplitude should then vary as the seismic moment at low frequencies. We have a rough idea of the position of the expected corner frequency as a function of magnitude from Atkinson and Boore (1995).

The essential step is to define a coda Green's function, which is the frequency-dependent shape of the coda for a flat moment-rate spectrum. Because we did not use very small earthquakes, which can define the high-frequency shape of the Green's function, we carefully did the following to define a Green's function for an $Mw = 4.0$ earthquake with an infinite corner frequency event. At the lower frequencies, we adjusted the coda levels for the differences in the $\log_{10}M_0$, using the three smallest events as a guide. This defined the coda Green's function shape to frequencies up to 4.0 Hz. We used the coda shape of the largest earthquake for $f \geq 4.0$ Hz to define the high-frequency shape by assuming that the source spectrum falls off as f^{-2}. After construction of this Green's function shape for an $Mw = 4.0$ ($\log_{10}M_0 = 22.10$), the spectral shapes of the events are all obtained (Figure 14).

For reference in Figure 14, we also plot the source spectral shapes for the Atkinson and Boore (1995) and the Frankel *et al.* (1996) source spectrum shapes as lightly dashed and solid curves, respectively. These two models seem to work well for the three largest earthquakes, but there may be a breakdown in the assumption of similarity for the smaller events. The conclusion drawn from this minimal sampling of available data from this earthquake sequence is that a detailed source spectral scaling study of this earthquake sequence is possible. The addition of waveforms from other stations and from smaller earthquakes will yield smoother estimates of the spectral scaling. We note, however, that the underlying assumption of this approach is that the frequency-dependent site effects do not change, and that the small differences in event depth do not significantly affect the relation between source moment and the generated coda signal.

INTERESTING WAVE PROPAGATION

Although wave propagation in the region shown in Figure 2 is such that a simple crustal velocity model suffices for broadband moment tensor inversion, there are significant departures from the model that are readily apparent in the observed waveforms. Within 500 km of the earthquakes, the strongest geological feature is the Mississippi embayment, a Cretaceous basin filled by fluvio-marine sediments with total sediment thickness increasing from a few tens of meters at the confluence of the Ohio and Mississippi Rivers at Cairo, Illinois, to about 900 meters near Memphis, Tennessee.

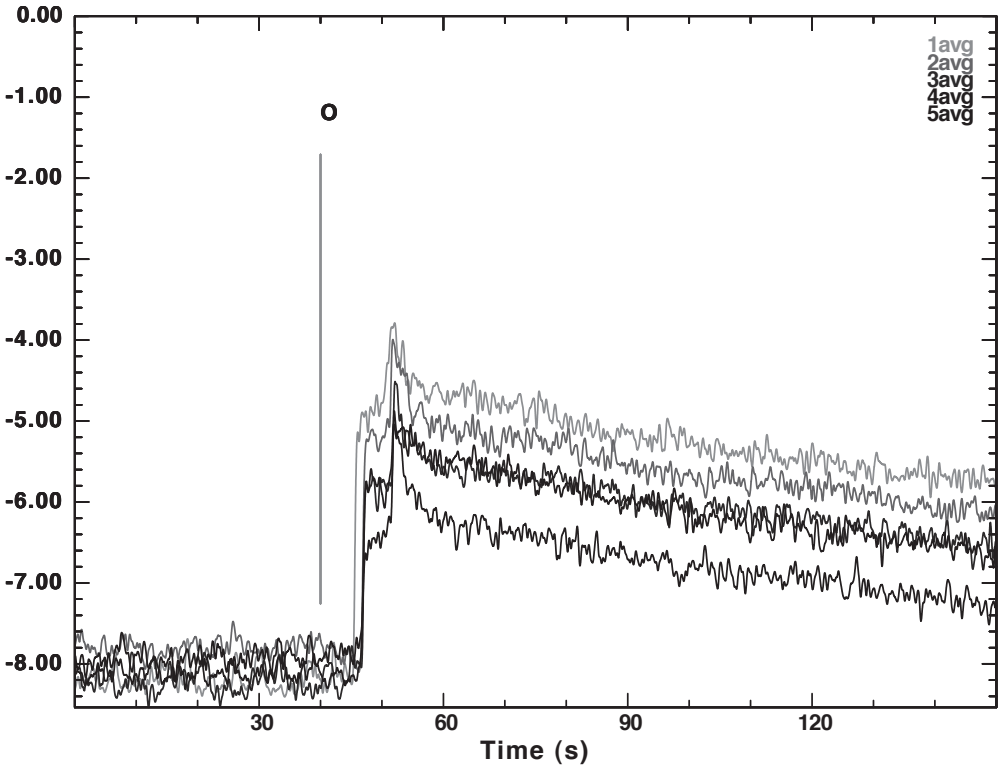

▲ **Figure 12.** Coda envelopes for 10–20 Hz frequency band plotted as a function of travel time. The events are ordered by decreasing moment magnitude. Note that the coda of events 3 and 4 overlie each other.

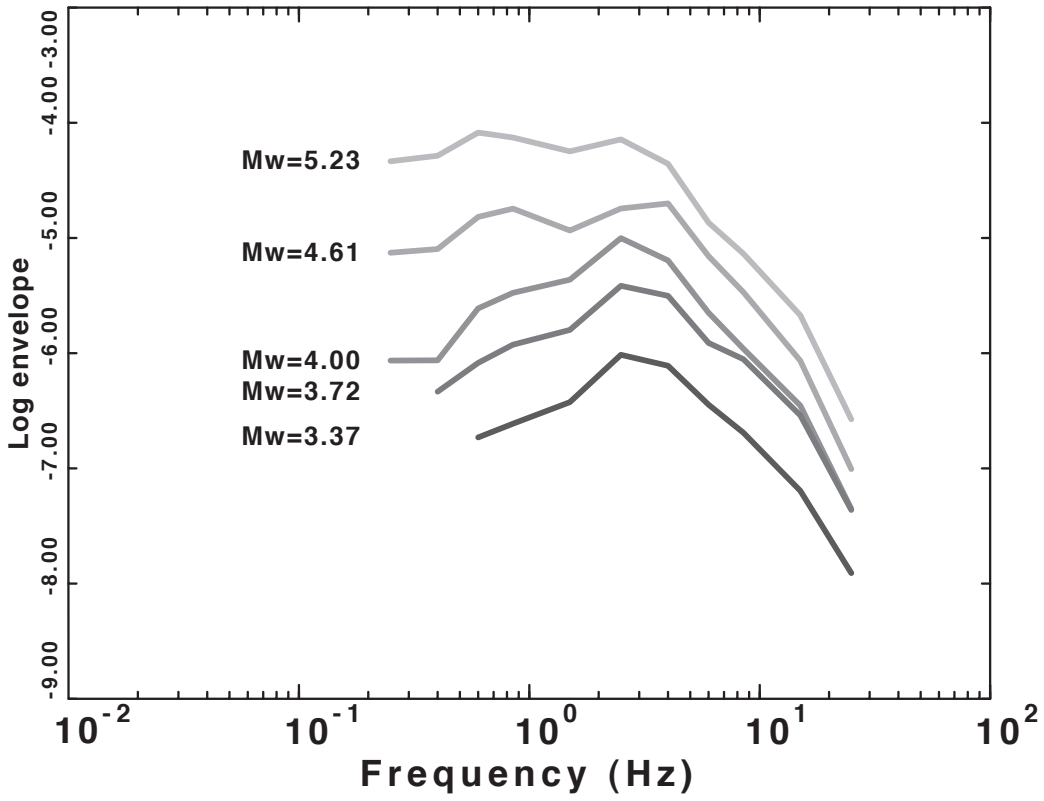

▲ **Figure 13.** Coda levels for the time window 90–110 s after the origin time.

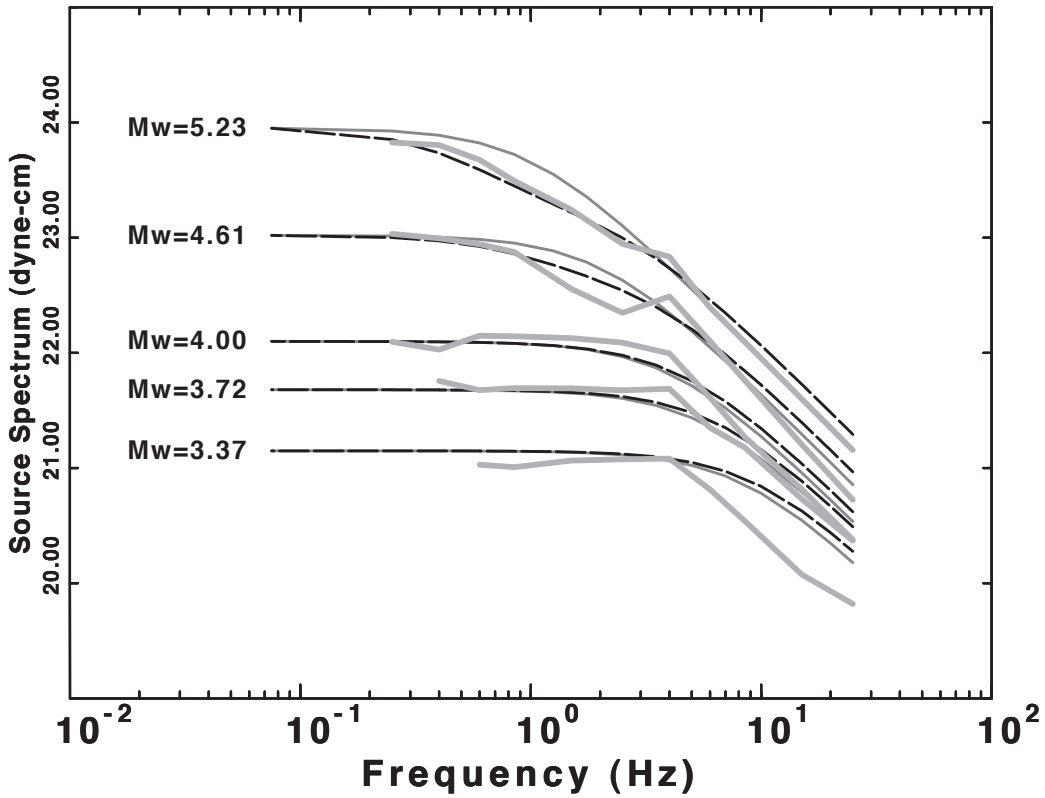

▲ **Figure 14.** Comparison of coda derived moment rate spectra (wide gray curves) and predicted scaling relations (thin gray line = Frankel *et al.* 1996; dashed line = Atkinson and Boore 1995) for the five earthquakes with known moment magnitude.

Wave propagation effects occur because of the thick deposits of low-velocity sediments overlying hard rock. In a study of local earthquakes with a portable deployment, Andrews *et al.* (1985) were the first to observe wave-type conversions from *P* to *Ps* and from *S* to *Sp* at the sharp rock–sediment interface. Bodin and Horton (1999) observed variations in the period of the peaks in the horizontal to vertical spectral ratios of microtremor measurements that are related to the spatial variations in the total sediment thickness. Direct observations of the sediment resonance effect were observed from broadband recordings at the University of Memphis of the 29 April 2003 Fort Payne, Alabama, earthquake (*cf.* reference 2 in Table 1).

Figure 15 compares observed and modeled filtered ground velocities (0.02–0.2 Hz) for the 18 April 09:37 main event at selected stations to the southwest of the earthquake. The stations HENM, PVMO, PBMO, and MPH are 237, 276, 291, and 411 km from the earthquake. The station PBMO lies just outside the embayment, while the thickness of the sediment column to the Paleozoic–Upper Cretaceous boundary is 500 m at HENM, approximately 600 m at PVMO, and 900 m at MPH (Julià *et al.* 2004). Examining the transverse components, we see that the initial part of the *S*-wave arrival is matched well in shape and amplitude by the predictions of the CUS model. However, a reverberation follows with period related to the sediment thickness and the mean shear-wave velocity of the sediment column. Such behavior can be modeled with a simple 1-D model. The vertical and especially the radial component signals for the stations in the embayment are more complicated. This may be due to multipathing affecting the near-nodal signals, the inherent complexity of *P-SV* motion, the effect of Rayleigh wave conversion into additional signals at the embayment edge, or some combination of factors. The resonance behavior at these periods has been observed for other earthquakes whose ray paths enter the embayment and may be important for the design of large structures with low natural frequencies.

DISCUSSION

This paper highlights the rich dataset available from what was in fact a moderate earthquake sequence, made possible by the investment in high-quality digital data acquisition in the area. We did not focus on detailed research results but rather pointed out the possibilities for further research in ground-motion scaling and crustal structure. The monitoring systems performed extremely well for this event. Cooperation and communication among most ANSS components at the national and regional levels provided an extensive suite of well-calibrated products.

The earthquake also serves to highlight that there is still much work to be done to bring an advanced national seismic system to fruition. Many of the installed monitoring systems do not yet meet ANSS performance specifications with respect to amplitude, frequency, time, or station location. Significant investments in communications infrastructure, modern hardware, software, and human resources are required to support the level of performance needed to provide rapid products for public safety and research products for scientists

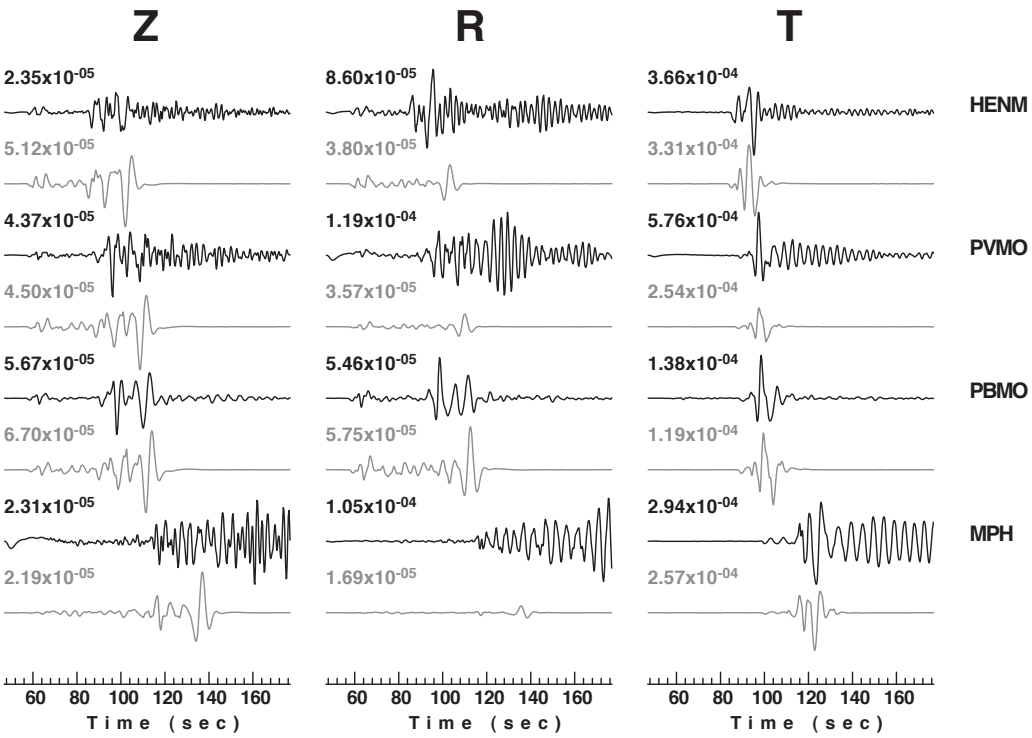

▲ **Figure 15.** Comparison of observed (black) and predicted (gray) waveforms for the main event at selected stations. See Figure 5 for figure details.

and engineers after the next large earthquake in the central and eastern U.S.

A collection of waveforms and instrument responses for the mainshock and some of the aftershocks is available at http://www.eas.slu.edu/Earthquake_Center/Significant_Earthquakes.html.

ACKNOWLEDGMENTS

This monitoring effort was sponsored in part by USGS awards 07HQAG0122 (SLU) and 07HQAG0019 (CERI), Saint Louis University and the University of Memphis. The success of the monitoring effort relies on the competent technical staffs at both institutions: E. Haug, R. Wurth, and M. Whittington at SLU and H. Withers, S. Brewer, J. Bollwerk, P. Lane, C. McGoldrick, B. Meiser, J. Parker, A. Sedaghat, D. Steiner, and G. Steiner at UM. GMT software (Wessel and Smith 1991) was used to create the maps.

REFERENCES

Aki, K. (1980). Attenuation of shear waves in the lithosphere for frequencies from 0.05 to 25 Hz. *Physics of the Earth and Planetary Interiors* **21,** 50–60.

Andrews, M. C., W. D. Mooney, and R. P. Meyer (1985). The relocation of microearthquakes in the northern Mississippi embayment. *Journal of Geophysical Research* **90,** 10,223–10,236.

Atkinson, G. M., and D. M. Boore (1995). New ground motion relations for eastern North America. *Bulletin of the Seismological Society of America* **85,** 17–30.

Bodin, P., and S. Horton (1999). Broadband microtremor observation of basin resonance in the Mississippi embayment, central U. S. *Geophysical Research Letters* **26,** 903–906.

Dziewonski, A., S. Bloch, and M. Landisman (1969). A technique for analysis of transient seismic signals. *Bulletin of the Seismological Society of America* **59**, 427–444.

Frankel, A., A. McGarr, J. Bicknell, J. Mori, L. Seeber, and E. Cranswick (1990). Attenuation of high-frequency shear-waves in the crust: Measurements from New York State, South Africa and southern California. *Journal of Geophysical Research* **95,** 17,411–17,457.

Frankel, A., C. Mueller, T. Barnhard, D. Perkins, E. Leyendecker, N. Dickman, S. Hanson, and M. Hopper (1996). *National Seismic Hazard Maps: Documentation June 1996.* USGS Open File Report 96-532, 69 pps.

Gordon, D. W. (1983). Revised hypocenters and correlation of seismicity and tectonics in the central U.S. PhD. dissertation, Saint Louis University, St. Louis, MO.

Herrmann, R. B. (1973). Some aspects of band-pass filtering of surface waves. *Bulletin of the Seismological Society of America* **63**, 663–671.

Herrmann, R. B. (1979). Surface wave focal mechanisms for eastern North America with tectonic implications. *Journal of Geophysical Research* **84,** 3,543–3,552.

Herrmann, R. B., and C. J. Ammon (2002). Computer programs in seismology, source inversion. http://www.eas.slu.edu/People/RBHerrmann/CPS330.html.

Julià, J., R. B. Herrmann, C. J. Ammon, and A. Akinci (2004). Evaluation of deep sediment velocity structure in the New Madrid seismic zone. *Bulletin of the Seismological Society of America* **94,** 334–340.

Kim, W. Y. (2003). The 18 June 2002 Caborn, Illinois earthquake: Reactivation of ancient rift in the Wabash Valley seismic zone? *Bulletin of the Seismological Society of America* **93,** 2,201–2,211.

Mayeda, K., A. Hofstetter, J. L. O'Boyle, and W. R. Walter (2003). Stable and transportable regional magnitudes based on coda-derived

moment-rate spectra. *Bulletin of the Seismological Society of America* **93,** 224–239.

Munson, P. J., S. F. Obermeier, C. A. Munson, and E. R. Hajic (1997). Liquification evidence for Holocene and latest Pleistocene seismicity in the southern halves of Indiana and Illinois: A preliminary overview. *Seismological Research Letters* **68,** 521–536.

Nuttli, O. W., and K. G. Brill (1981). Earthquake source zones in the central United States determined from historical seismicity. In *Approach to Seismic Zonation for Siting Nuclear Electric Power Generating Facilities in the Eastern United States*, ed. N. L. Barstow, K. G. Brill, O. W. Nuttli, and P. W. Pomeroy, 98–143. Washington, DC: U. S. Nuclear Regulatory Commission Report NUREG/CR-1577.

Odum, J. K., W. J. Stephenson, R. A. Williams, and D. M. Worley (2005). Examples of site characterization and *Vs30* measurements at ANSS stations at selected sites across the United States. *Seismological Research Letters* **76** (2), 232.

Odum, J. K, R. A. Williams, W. J. Stephenson, and D. M. Worley (2008). Shallow seismic velocity and *Vs30* at ANSS sites in Southern Illinois and Evansville, Indiana. (in review).

Taylor, K. B., R. B. Herrmann, M. W. Hamburger, G. L. Pavlis, A. Johnston, C. J. Langer, and C. Lam (1989). The southeastern Illinois earthquake of 10 June 1987. *Seismological Research Letters* **60,** 101–110.

U.S. Geological Survey (1999). *An Assessment of Seismic Monitoring in the United States: Requirement for an Advanced National Seismic System*. USGS Circular 1188, 55 pps. Available at http://pubs.usgs.gov/circ/1999/c1188/ .

Wang, C. Y., and R. B. Herrmann (1980). A numerical study of *P-*, *SV-* and *SH*-wave generation in a plane layered medium. *Bulletin of the Seismological Society of America* **70,** 1,015–1,036.

Wessel, P., and W. Smith (1991). Free software helps map and display data. *Eos, Transactions, American Geophysical Union* **72,** 441, 445–446.

Zhu, L., and D. V. Helmberger (1996). Advancement in source estimation techniques using broadband regional seismograms. *Bulletin of the Seismological Society of America* **86,** 1,634–1,641.

Department of Earth and Atmospheric Sciences
Saint Louis University
3642 Lindell Boulevard
St. Louis, Missouri 63108 USA
rbh@eas.slu.edu
(R. B. H.)
mwithers@memphis.edu
(M. W.)
benz@usgs.gov
(H. B.)